Purging of dropwise condensate by electrowetting

J. Kim and M. Kaviany[a)]
Department of Mechanical Engineering, University of Michigan, Ann Arbor, Michigan 48109-2125

(Received 12 November 2006; accepted 20 March 2007; published online 23 May 2007)

The onset of motion of a dropwise condensate (on inclined substrate) under applied direct current potential (with an overhanging electrode) is studied experimentally and described based on overcoming of the static three-phase contact line (TCL) friction by electrowetting. Electrowetting phenomenon exerts a radial electrostatic force on the TCL, causing an imbalance in the TCL surface tension forces, thus initiating the surface droplet motion (by an applied threshold, local electric field intensity). The experimental results using overhanging wire electrodes have identified three regimes (gravity dominated, intermediate, and surface force dominated) and show significant lowering of the critical inclination angle for the liquid droplet. In the intermediate Bond number regime (both gravity and surface liquid-gas tension are significant), the critical (for onset of motion) electrostatic potential is predicted and good agreement is found with experiments. © *2007 American Institute of Physics*. [DOI: 10.1063/1.2734933]

I. INTRODUCTION

Water surface drops with volume of the order of microliter (mL) (placed or condensed) form a well defined three-phase contact line (TCL) and contact angle. Then the contact line friction contributes substantially in surface droplet dynamics.[1,2] Since the classical hydrodynamics cannot fully describe the motion of the TCL, several strategies have been introduced to resolve the problem.[3–5] However, these approaches have been exclusively for dynamic analysis by estimating the friction force as a product of the friction coefficient and the velocity of the contact line. Little is known about the static contact line friction just prior to initiation of TCL motion. Nevertheless, since liquid droplets, unlike solid objects, undergo significant topological changes in response to external forces, it is possible to estimate the force necessary to initiate motion of the TCL by examining the topological observables (local radius meniscus curvature, local contact angle, etc.) at the critical inclination angle.

One of the observables used for estimating the force acting on a liquid droplet is the contact-angle hysteresis (difference between the advancing and receding contact angles). This is a complex topological feature since it represents contact line friction and surface forces in response to an external force acting on the droplet volume. Thus, the contact angle hysteresis is extensively used to analyze the force acting on droplets for both surface-force dominated (microscale liquid droplet management)[6] and the gravity-dominated (heat exchanger condensation management)[7,8] systems. So, two distinct approaches have been used to describe the dominated forces, i.e., the surface-electrostatic and surface-gravity. However, the cases of three or more forces, which include liquid volumes of the order of tens of μL, have not been examined.

Dropwise condensation occurs when moist air flows in refrigeration or air-conditioning heat exchangers and can block the air passage and degrade the performance, thus requiring periodic water surface droplet or frost purging.[9–11] Surface modifications have been devised to reduce the critical angle at which a given volume surface droplet begins to slide under gravity. These include the recent study achieving a 50% reduction in the volume needed for the onset of droplet sliding, using a microgrooved (directional) aluminum surface. However, these passive surface modification techniques are not suitable for versatile operating conditions and active control of the condensate. Here we examine (theoretically and experimentally), for the first time, purging of surface droplets by electrowetting, a phenomenon based on the interaction of the electrostatic, gravity, and surface forces. Experimental data for the critical angle (for onset of droplet motion) are presented along with a theoretical description using a one-dimensional force balance at the TCL based on macroscopic droplet topological observables. We aim to close the existing gap between the two distinct field of research involving microscale liquid droplet management and heat exchanger condensate management.

II. THEORETICAL BACKGROUND

Liquids form a spherical cap with a well-defined equilibrium contact angle $\theta_{c,o}$ or spread across the surface as a thin film when condensed or injected onto a solid surface. The precise equilibrium that determines the topology of droplet is the balance between the liquid-gas σ_{lg}, solid-liquid σ_{sl}, and gas-solid σ_{gs} interfacial tensions. This balance of forces is represented by the free energy at the contact line

$$F_{if} = \sum A_i \sigma_i - \lambda V, \tag{1}$$

where λ is the Lagrangian multiplier for the constant volume constraint, A is area, and λ is equal to the capillary pressure Δp across the liquid-gas interface. Minimization of the free energy leads the following two conditions which govern the topology (meniscus) of the droplet.[12,13] The first is the meniscus Laplace equation which states that Δp is constant over the entire interface

[a)]Author to whom correspondence should be addressed; electronic mail: kaviany@umich.edu

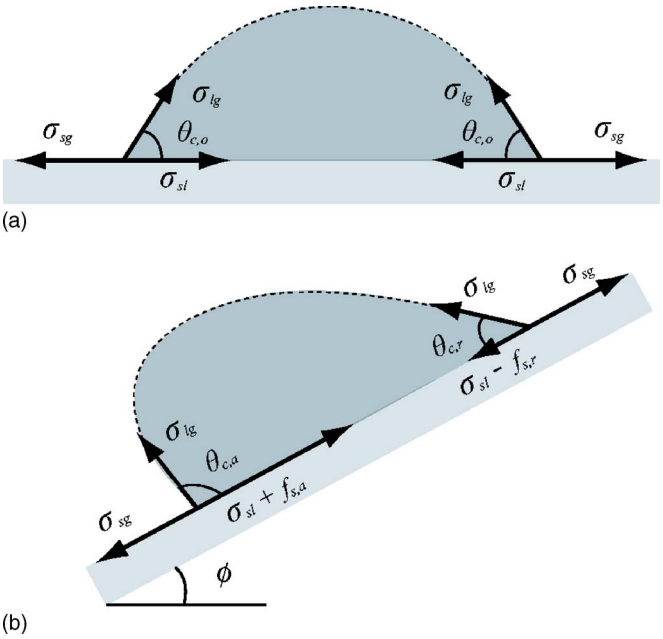

FIG. 1. (a) Balance of forces at the TCL for $\phi=0°$ and (b) for $\phi>0°$.

$$\Delta p = \sigma_{\mathrm{lg}}\left(\frac{1}{r_1}+\frac{1}{r_2}\right), \tag{2}$$

where r_1 and r_2 are the two principal radii of curvature of the meniscus. The Laplace equation shows that for homogeneous substrates, liquid droplets adopt a spherical cap shape in mechanical equilibrium. The other is the contact line Young equation

$$\cos\ \theta_{c,\,o} = \frac{\sigma_{\mathrm{sg}}-\sigma_{\mathrm{sl}}}{\sigma_{\mathrm{lg}}}. \tag{3}$$

This relates the interfacial tension to the apparent contact angle $\theta_{c,\,o}$. Figure 1(a) shows the contact angle and the surface tension in equilibrium for the liquid droplet on a horizontal surface. For the relevant scale, often, it is possible to adopt a one-dimensional model of the contact line, where the three interfacial tensions are pulling on the TCL.

For a liquid on an inclined surface, the ratio of the surface forces to gravity is represented by the Bond number ($\mathrm{Bo}=\rho g D^2 \sin\phi/\sigma_{\mathrm{lg}}$). We consider moderate Bond numbers ($\mathrm{Bo}=0.8-2.5$), so the droplet motion is influenced by gravity (but not dominated). For a plate inclination angle ϕ, the mass center of the droplet shifts toward the advancing side, giving rise to the local capillary pressure Δp at the liquid-gas interface. The opposite phenomenon exits on the receding side. The TCL of the advancing side is pinned due to the contact line friction and is not allowed to advance until a critical inclination angle is reached. Then at the advancing side, according to Eq. (2), reduction in the radius of curvature occurs and the contact angle to increase. At the receding side, reduction of the local capillary Δp requires a larger radius of curvature and this results in a smaller contact angle. This difference between the advancing and receding contact angles is referred to as the contact angle hysteresis and is shown in Fig. 1(b). As seen in the figure, the force balance at the TCL is modified due to the presence of contact line friction. From the point of the surface tension equilibrium at the TCL, the contact angle hysteresis can be modeled as the addition of friction, f_s (per unit length), to the σ_{ls} at the advancing side and subtraction of friction, f_s, at the receding side. The radial component of f_s varies along the azimuthal angle ς, thus, the contact angle varies from $\theta_{c,\,a,\,\mathrm{max}}$ to $\theta_{c,o}$ then to $\theta_{c,r,\mathrm{min}}$.

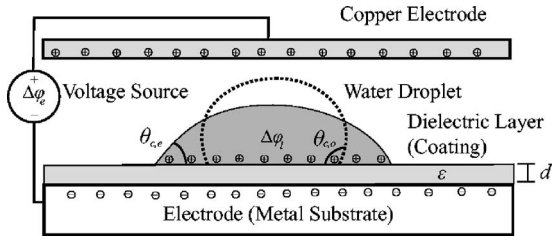

FIG. 2. Rendering of electrowetting of the surface droplet on a dielectric coated substrate.

The contact angle hysteresis and the retention force (the sum of f_s over the entire contact line) can be related using the following equation for circular droplets:[14,15]

$$F_s = k\sigma_{\mathrm{lg}}R(\cos\ \theta_{c,r}-\cos\ \theta_{c,a}), \tag{4}$$

where k is a constant, R is the length scale representing the size of the meniscus, and $\theta_{c,r}$ and $\theta_{c,a}$ are the receding and advancing contact angles. k depends on the topology of the droplet and is found empirically using the measured receding and advancing contact angles at the critical inclination angle. Knowing k and using the droplet force balance, the critical inclination angle can be found. However, measuring the advancing and receding contact angles at the critical condition is challenging.[16,17] These references perform a comprehensive empirical analysis of droplets on aluminum substrates, with commercially available coatings. They propose an empirical relation between the Bond number and the ratio of the receding and advancing contact angles, i.e.,

$$\frac{\theta_{c,a}}{\theta_{c,r}} = 0.01\ \mathrm{Bo}^2 - 0.155\ \mathrm{Bo} + 0.97. \tag{5}$$

This relationship is used to estimate the retention force over the entire range of Bond numbers.

Electrowetting has become an active field of research for various applications in microfluidics, where surface forces dominate. Figure 2 renders the contact angles affected by electrowetting. Extensive research has been done with spatial dimensions where gravity effects are negligible (Bond number tending to zero).[18–20] However, for moderate Bond numbers, the electrowetting literature is not as rich.

To relate the applied voltage to the change in the effective surface tension, the thermodynamic-electrochemical, energy minimization, and electromechanical approach have been used.[7,21–23] All of these approaches converge to a single well-accepted electrowetting relation which is presented later. Here the electromechanical approach first introduced in Ref. 22 is used and starts from the Korteweg–Helmholtz body force density[24]

$$\mathbf{F}_k = \rho_f \mathbf{E} - \frac{\varepsilon_0}{2} E^2 \nabla \varepsilon + \nabla\left(\frac{\varepsilon_0}{2} E^2 \frac{\partial \varepsilon}{\partial \rho} \rho\right), \tag{6}$$

where ρ_f and ε are the mass density and the dielectric constant of the liquid. The last term in Eq. (6) describes the electrostriction and can be neglected. If we assume that the liquid is perfectly conductive, integrating Eq. (6) over the entire volume is equivalent to integrating the Maxwell stress tensor over the liquid-gas interface

$$\mathbf{F}_e = \oint \mathbf{T} \cdot \mathbf{n}\, ds, \tag{7}$$

where $\mathbf{T}$ is the Maxwell stress tensor, which is written as

$$\mathbf{T}_{ik} = \varepsilon_o \varepsilon\left(-\tfrac{1}{2}\delta_{ik}|\mathbf{E}|^2 + \mathbf{E}_i \mathbf{E}_k\right), \tag{8}$$

where δ_{ik} is the Kronecker delta. The tangential component of the electric field at the surface vanishes and the normal component is related to the local surface charge density through $\rho_s = \varepsilon_o \mathbf{E} \cdot \mathbf{n}$. Now noting that every term except the component directed along the outward surface normal vanishes, Eq. (7) becomes

$$\mathbf{F}_e = \oint \frac{1}{2} \rho_s \mathbf{E}\, ds. \tag{9}$$

The field and charge distribution are found by solving the electrical Laplace equation for the electrostatic potential with the appropriate boundary conditions. It was found that both the field and charge distributions diverge upon approaching the contact line.[25] Therefore, the Maxwell stress in maximum at the contact line and exponentially decays with distance from the contact line. After integration, the horizontal component of the Maxwell stress is

$$f_e = \frac{\varepsilon_o \varepsilon}{2d} \Delta\varphi^2. \tag{10}$$

Since this force acts only on the contact line and is perpendicular to the TCL, it is used in the force balance and the Young equation, i.e.,

$$\sigma_{\mathrm{sl},e}^{\mathrm{eff}} = \sigma_{\mathrm{sl}} - \frac{\varepsilon_0 \varepsilon}{2d} \Delta\varphi^2, \tag{11}$$

$$\cos\,\theta_{c,e} = \cos\,\theta_{c,o} + \frac{\varepsilon_0 \varepsilon}{2\sigma_{\mathrm{lg}} d} \Delta\varphi^2, \tag{12}$$

where $\theta_{c,e}$ is the electrowetted contact angle, $\theta_{c,o}$ is the neutral contact angle, ε is the dielectric constant of the dielectric layer underneath the water droplet, d is the thickness of the dielectric layer, and $\Delta\varphi$ is the applied potential between the liquid and the electrode underneath the dielectric layer. Ideally, as the potential is increased, the electrowetted contact angle approaches zero. However, it is found that the contact angle saturates at a value $\theta_{c,\mathrm{sat}}$ varying between 30° and 80°, depending on the system.[26,27] This contact angle saturation can be explained as an electron-discharge mechanism,[20] together with the vertical component of the electrostatic force acting on the contact line.[28]

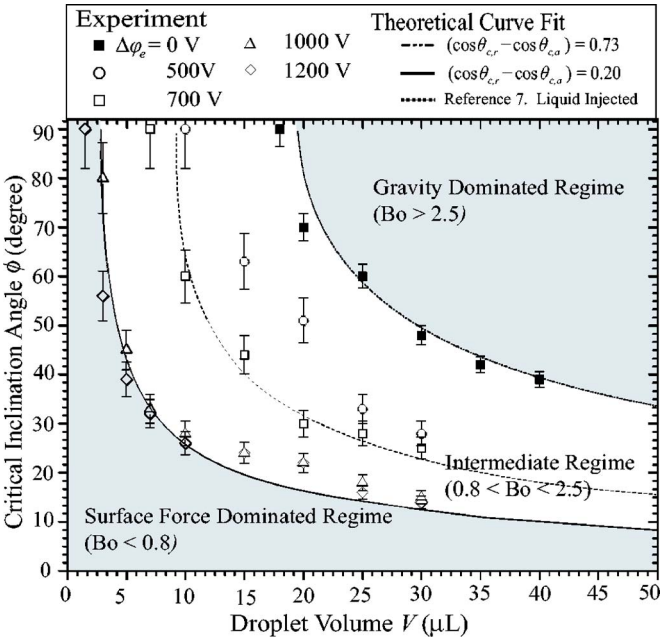

FIG. 3. Variation of the critical inclination angle with respect to the droplet volume for applied potential $\Delta\varphi$=500, 700, 1000, and 1200 V. The curve was fitted using the force balance between gravity and the retention force $\phi = \sin^{-1}\{[1.845\sigma_{\mathrm{lg}}(\cos\,\theta_{c,r} - \cos\,\theta_{c,a})]/\rho g V\}$.

III. EXPERIMENT

Experiments were conducted to investigate the electrowetting induced purge for liquid droplet on an inclined substrate. A 30 mm × 30 mm cold rolled aluminum alloy 1100 was coated with a dielectric layer (polymer-based electric insulation coating ε=2.4 and $\theta_{c,o}$=70°) with 200 μm in thickness. A second polymer-based P4 (ε=3.0 and $\theta_{c,o}$ =110°) hydrophobic coating (Circle Prosco, Bloomington, IN) with 300 μm in thickness was coated on top of the first layer. Using a μL syringe, de-ionized water droplet was placed on the hydrophobic substrate. Then the substrate was tilted to find the baseline (no applied electric potential) where the water droplets begin to slide due to gravity. Subsequently, the electric potentials of 1200, 1000, 700, and 500 V were applied from the overhanging electrode. The wire electrode (0.5 mm in diameter) was brought as close to the water droplet, without touching it. Then the angle at which the water droplet starts to slide was recorded. The experiment was photographed using a DSLR camera with a 1:1 macrolens. In addition, experiments with a fixed overhanging plate electrode were conducted in order to explore the possibility of implementation in a heat exchanger. A P4 hdydrophobic coated copper panel (100 μm in thickness) was used.

IV. RESULTS AND DISCUSSION

Figure 3 shows the variation of the critical inclination angle with respect to the liquid droplet volume, for different applied potentials. The base line with no applied voltage is shown by the dashed line which was found to follow a line with Bo=2.5. The figure shows that electrowetting significantly reduces the critical angle of inclination of liquid water droplet. At an applied potential larger than 1000 V (Bo =0.8 is represented by the solid line), no significant change

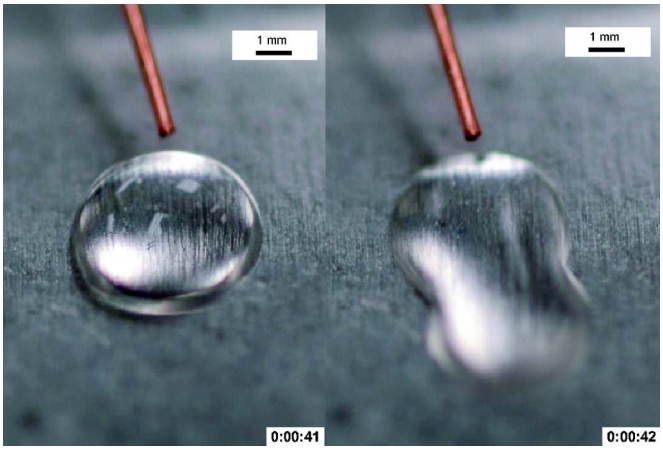

FIG. 4. Images of the advancing contact line before and right after the onset of motion (V=10 μl, $\Delta\varphi$=700 V, ϕ=60°).

in the critical inclination angle is found, indicating saturation. The results shows that there exist three distinct regimes, namely, above Bo=2.5 and below Bo=0.8 where gravity and surface forces dominate, respectively, and an intermediate (moderate) Bo regime where the critical inclination angle varies with the applied potential. In the moderate Bo regime, the gravity, electrostatic, and surface forces are at all of the same order of magnitudes and are in balance and the critical inclination angle depends on the applied potential.

The critical inclination angle at an applied potential was found to follow the constant Bo line which suggests that the electrostatic force reduces the contribution of the surface forces. At the critical inclination angle (under electrowetting), a significant contact line slip of the advancing side was observed, as shown in Fig. 4. When the advancing contact line begins to slip, no slip was observed on the receding contact line until the advancing side had well advanced. At high potentials, above 2000 V, the advancing side of the liquid droplet detaches from the receding side due to instability. The images from the side and top of the advancing droplet are shown in Figs. 5(a) and 5(b).

In order to analyze the earlier experimental observations, a simple force balance is used at the TCL. At the TCL, a force of $f_e=(\varepsilon_o\varepsilon/2d)\Delta\varphi^2$ per unit length is applied in the radial direction as predicted by Eq. (10). As a result, the x component of the electrowetting force will vary as the cosine of the azimuthal angle ς. In contrast, the contact line friction is constant along the TCL in the x direction. Note that the integral of the contact line friction at the critical inclination angle is equal to the retention force, which is given by Eq. (4). The value of k for the presented experiment was found to be 1.845. Then according to the classical droplet mechanics and by using the retention force data, the sum of the forces at the critical inclination angle can be written as

$$F_x = \int_{-\pi/2}^{\pi/2} 2Rf_e \cos\zeta d\zeta - \frac{1}{2}F_{sx}$$

$$= \int_{-\pi/2}^{\pi/2} R\frac{\varepsilon_o\varepsilon}{d}\Delta\varphi^2 \cos\zeta d\zeta - 0.923\sigma_{lg}R(\cos\theta_{c,r} - \cos\theta_{c,a}). \quad (13)$$

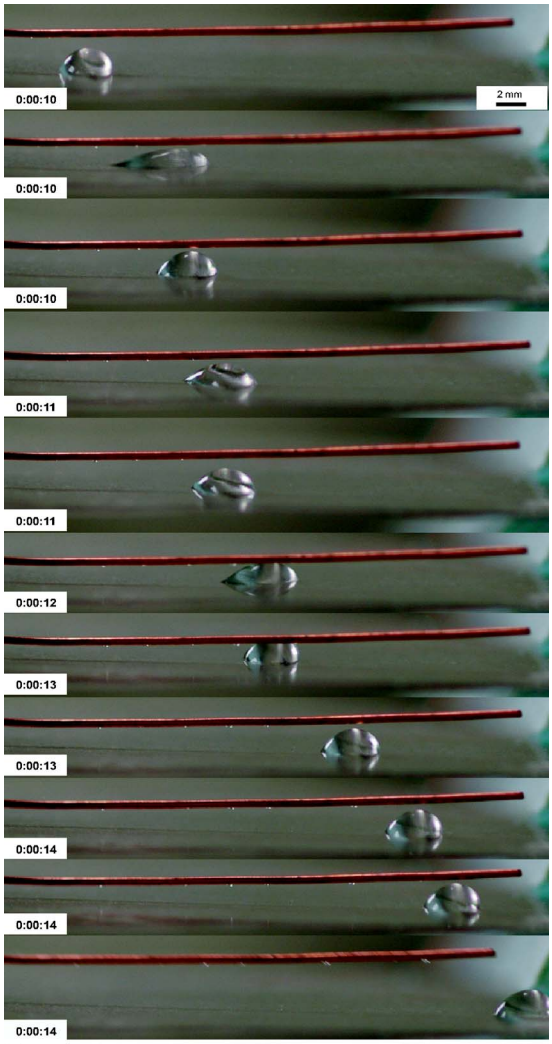

(a)

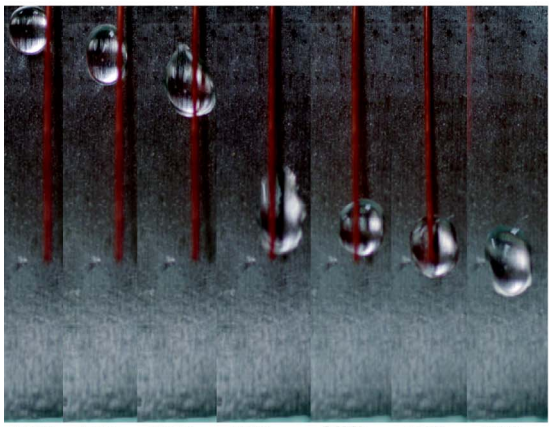

(b)

FIG. 5. (a) Side image of surface droplet advancement (V=4 μl, $\Delta\varphi$ =1000 V, ϕ=50°) and (b) top image of the same.

We have assumed that the applied forces are concentrated at the TCL, as graphically represented in Fig. 6. It can be seen graphically that the contact line of the advancing side will start to slip when the electrowetting overcomes the local static contact line friction value at the location of $\theta_{c,a,\max}$ along the TCL. As f_e becomes larger with increase in potential, the portion of the contact line which begin to

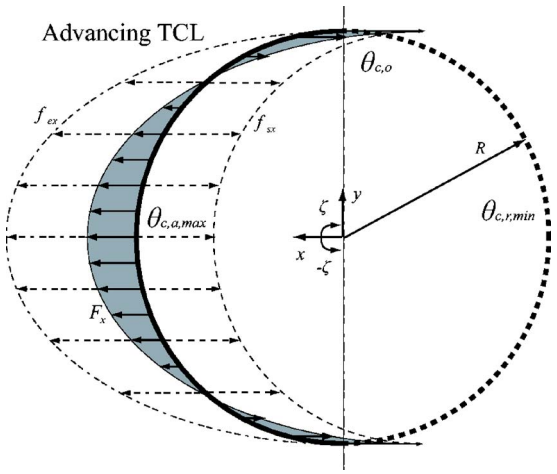

FIG. 6. Graphical representation of balance between the retention and electrowetting forces, at the advancing TCL.

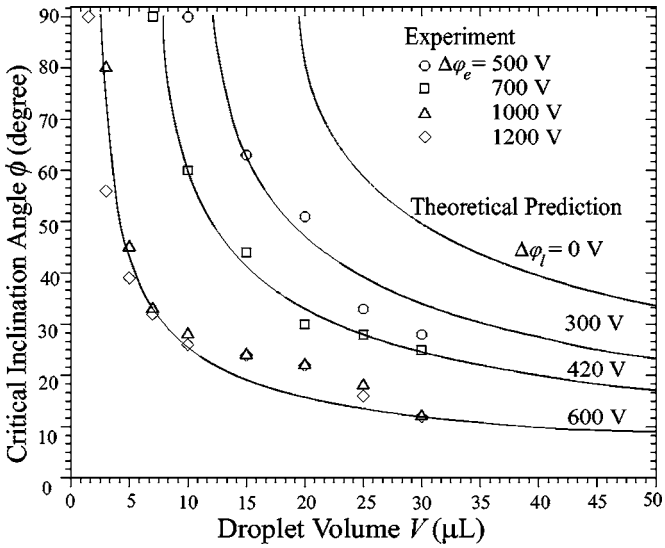

FIG. 7. Variation of the critical inclination angle with respect to condensate volume. Here $\Delta\varphi_e$ is the measured electrode potential and $\Delta\varphi_l$ is the predicted droplet potential. The experiment results are averaged (over several experiments) values.

slip increases. Also, as the contact line begins to slip, it causes an instantaneous reduction in the advancing contact angle. When the advancing contact angle is reduced, according to Eq. (12), the retention force is reduced which results in lowering of the critical inclination angle (for the given liquid volume). The exact relationship between the instantaneous contact angle reduction and the retention force is expected to be complex and is not addressed here. When a sufficient portion of the contact line friction is removed, the bulk liquid motion is initiated. It was observed that for the tested substrate, the contact line slip is initiated at approximately 300 V. However, the bulk motion of the water droplet was not observed until the applied voltage of 400 V was reached.

When the droplet is in motion, its periodic wetting and dewetting was observed as seen in Fig. 5(a). We suspect that continuous charging and discharging of the water droplet occurs while the droplet is in motion. The motion can be described as a sequence where first, at the onset of motion, the droplet is charged and experiences electrowetting which overcomes the static TCL friction. When the sum of the gravity and electrowetting force is larger than the static friction over the entire contact line of the droplet, the bulk condensate motion is initiated. As the droplet advances, the electrostatic energy is dissipated and dewetting becomes apparent. When the droplet recovers its original topology, it experiences a rise in electrostatic energy due to its proximity to the over-hanging electrode and this sequence is repeated.

We also predict the electrowetting reduction of the critical inclination angle by performing classical droplet mechanics. As mentioned earlier, the observation indicates that minimum or no advancing of the receding contact line until the advancing contact line has well advanced, thus, it is reasonable to assume that the dominate criteria for the initiation of the droplet motion is the force balance at the advancing contact line. As long as the droplet is not separated, this treatment of the force on the contact line is valid. The retention force can be estimated using Eq. (4) with the empirical contact angle relation (5). The electrowetting force can be calculated by integrating the x component acting on the TCL over the azimuthal angle for the advancing portion of the droplet. Then by solving for the inclination angle which the gravity balances, the resultant of the retention force and the electrowetting force, it is possible to obtain a theoretical prediction of the variation of the critical inclination angle with the applied potential. This angle is found by solving the following equation:

$$\phi = \sin^{-1}\left[\frac{\int_{-\pi/2}^{\pi/2} R\frac{\varepsilon_o \varepsilon}{d}\Delta\varphi^2 \cos\zeta d\zeta - 0.923\sigma_{\mathrm{lg}}(\cos\ \theta_{c,a} - \cos\ \theta_{c,r})}{\rho g V}\right]. \tag{14}$$

The theoretical predictions are presented in Fig. 7. It was found that when using Eqs. (4) and (10) and plotting the results, the required potential is 60% of the applied potential and was consistent for all four theoretical predictions. This discrepancy between the applied potential and the effective droplet potential can be traced back to the few assumptions that were made to perform the analysis. One of them is the assumption made in the force balance at the TCL using the elecrowetting equation which treats the electrostatic force as a surface (one-dimensional) force. Note that withstanding the

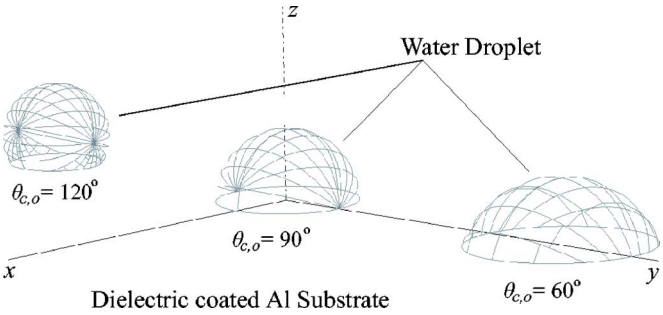

FIG. 8. Three-dimensional model of the water droplets with varying contact angles ($\theta_{c,o}$=120°, 90°, 60°) and on the Al substrate. ($\Delta\varphi_l$=1000 V, V =20 μl d=500 μm, ε=2.4.)

findings in Ref. 25, the force due to electrowetting is, in essence, a body force. Therefore, there exist discrepancies when the electrowetting force is treated as a surface force in formulating the force balance at the TCL. This discrepancy is more apparent at high potentials, such as those used here. Solving the Maxwell equations numerically (using solver Maxwell[29]), the results of the simulation are given in Figs. 8 and 9. The surface droplet is modeled as a spherical cap with a potential applied directly to the droplet. The aluminum substrate is coated with a dielectric layer (ε=2.4) of 500 μm. The results show that at the TCL, the diverging local electric field is not localized to an infinitesimal volume at the TCL, but instead extends along the liquid-gas interface. It was found that the higher the contact angle [Fig. 9(a)], the further extents this diverging field along the liquid-gas interface. This results in lower field intensity at the TCL. Although this analysis is not exact at the molecular,[30] nevertheless, it gives an insight into the discrepancy between the experimental results and the theoretical prediction.

V. CONCLUSIONS

Experimental investigation of electrowetting induced onset of surface droplet motion using overhanging electrode shows significant decrease in the critical inclination angle. The range of Bond number is between 2.5 and 0.8 and the applied potential is up to 1200 V. The electrowetting induces a droplet contact line slip at the advancing front which can be interpreted as alleviation of the contact line friction. Theoretical prediction is made by performing a force balance between the retention, gravity, and electrostatic forces at the advancing contact line, using the macroscopic topological observables. The theoretical analysis can be also be used when the surface and electrostatic forces (or the gravity and electrostatic forces) dominate. Identification of the intermediate region, where the critical inclination angle is a function of the applied electric potential, closes the gap between the surface-force dominated and gravity dominated regimes (under electrostatic force), thus allowing for manipulation of the condensate movement. This analysis may guide future investigations of the systems with combined surface, gravity, and electrostatic forces.

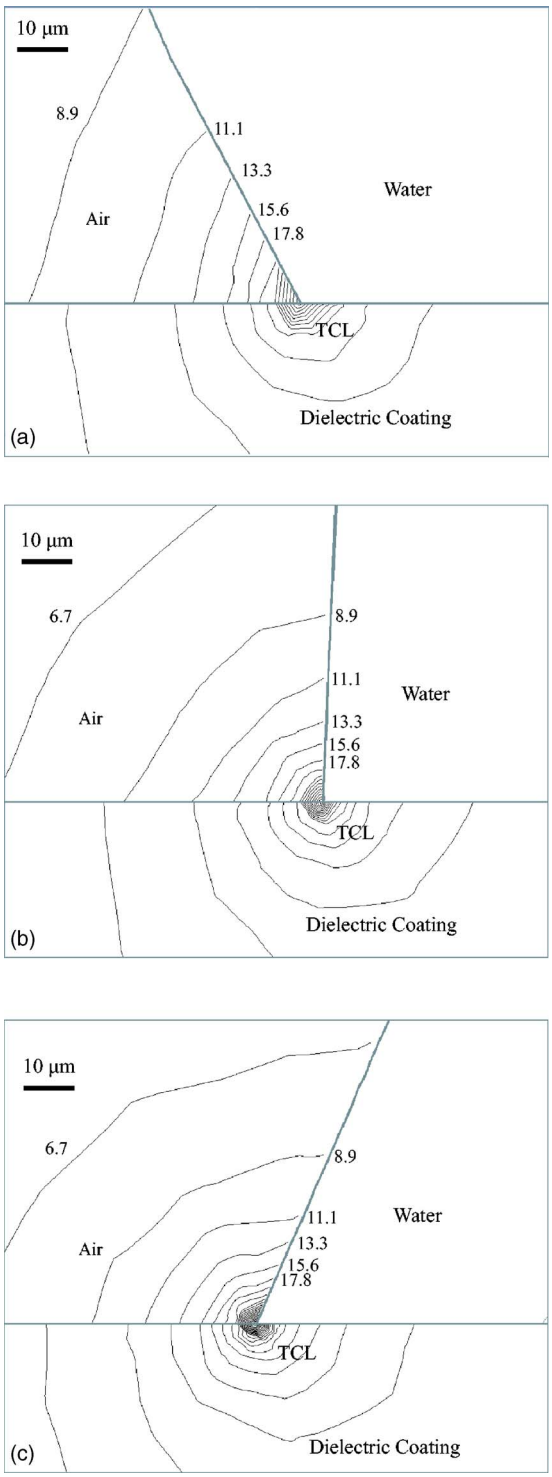

FIG. 9. Constant electric field lines (in 10^6 V/m) at the vicinity of the TCL. (a) $\theta_{c,o}$=120°, (b) $\theta_{c,o}$=90°, and (c) $\theta_{c,o}$=60°. The results are for $\Delta\varphi_l$ =1000 V, V=20 μl, d=500 μm, ε=2.4, and energy error of 0.006%.

ACKNOWLEDGMENTS

The authors are thankful for useful discussions with Hailing Wu, Michael Heidenreich, and Steve Wayne of Advanced Heat Transfer, LLC and Jeffrey Bainter of Circle Prosco, Inc.

[1]H. Ren, R. B. Fair, M. G. Pollack, and E. J. Shaughnessy, Sens. Actuators B **87**, 201 (2002).
[2]K. L. Wang and T. B. Jones, Langmuir **21**, 4211 (2005).

[3]P. G. deGennes, Langmuir **18**, 3413 (2002).
[4]L. M. Pismen, Colloids Surf., A **206**, 11 (2002).
[5]A. Oron, S. H. Davis, and S. G. Bankoff, Rev. Mod. Phys. **69**, 931 (1997).
[6]F. Mugele and J. C. Baret, J. Phys.: Condens. Matter **17**, R705 (2005).
[7]A. D. Sommers and A. M. Jacobi, J. Micromech. Microeng. **16**, 1571 (2006).
[8]J. Shin and S. Ha, Int. J. Refrig. **25**, 688 (2002).
[9]M. Kaviany, *Principles of Heat Transter* (Wiley, New York, 2001), Chap. 6, p. 646.
[10]B. Na and R. L. Webb, Int. J. Heat Mass Transfer **47**, 925 (2004).
[11]A. F. Emergy and B. L. Siegel, *AIAA/ASME Thermophysics and Heat Transfer Conference, Heat and Mass Transfer in Frost and Ice packed Beds and Environmental Discharges*, Seattle (1990), pp. 1–7.
[12]A. Adamson, *Physical Chemistry of Surfaces*, 4th ed. (Wiley, New York, 1982), Chap. 1, p. 8.
[13]J. N. Israelachvili, *Intermolecular and Surface Forces*, 1st ed. (Academic, San Diego, 1985), Chap. 9, p. 120.
[14]C. W. Extrand and Y. Kumagai, J. Colloid Interface Sci. **170**, 515 (1995).
[15]C. W. Extrand and A. N. Gent, J. Colloid Interface Sci. **138**, 431 (1990).
[16]A. I. Elsherbini and A. M. Jacobi, J. Colloid Interface Sci. **273**, 556 (2004).
[17]A. I. ElSherbini and A. M. Jacobi, J. Colloid Interface Sci. **273**, 566 (2004).
[18]V. Srinivasan, V. K. Pamula, and R. B. Fair, Lab Chip **4**, 310 (2004).
[19]B. Berge and J. Peseux, Eur. Phys. J. E **3**, 159 (2000).
[20]K.-S. Yun, I.-J. Bu, J.-U. Bu, C.-J. Kim, and E. Yoon, J. Microelectromech. Syst. **11**, 454 (2002).
[21]B. Berge, C. R. Acad. Sci., Ser. II: Mec., Phys., Chim., Sci. Terre Univers **317**, 157 (1993).
[22]T. B. Jones, Langmuir **18**, 4437 (2002).
[23]T. B. Jones, J. Micromech. Microeng. **15**, 1184 (2005).
[24]L. D. Landau and E. M. Lifschitz, in *Electrodynamics of Continuous Media* (Pergamon, Oxford, 1960), Chap. 15, p. 213.
[25]M. Vallet, M. Vallade, and B. Berge, Eur. Phys. J. B **11**, 583 (1999).
[26]V. Peykov, A. Quinn, and J. Ralston, Colloid Polym. Sci. **278**, 789 (2000).
[27]H. Moon, S. K. Cho, R. L. Garrell, and C. J. Kim, J. Appl. Phys. **92**, 4080 (2002).
[28]K. H. Kang, Langmuir **18**, 10318 (2002).
[29]Maxwell 3D ver. 10.0.14, Ansoft Corp., 1984–2003, electrostatic field simulator.
[30]J. Buehrle, S. Herminghaus, and F. Mugele, Phys. Rev. Lett. **91**, 086101 (2003).